Veröffentlichungen
Museum für Naturkunde
Chemnitz
45 2022 67–80

Water-rich coesite in prismatine-granulite from Waldheim/ Saxony

Wasserreicher Coesit im Prismatin-Granulit von Waldheim/ Sachsen

Rainer Thomas, Friesack, Paul Davidson, Hobart, Adolf Rericha, Falkensee & Ulrich Recknagel, Schrobenhausen

Abstract

In this paper, we studied very rare coesite-like crystals in prismatine granulite rock from Waldheim/Saxony with Raman spectroscopy. This coesite shows a clearly different Raman spectrum characterized by very strong bands at 272 and 339 cm^{-1}, in addition to the strong band between 521 and 528 cm^{-1}. In addition to these bands, a further strong band at about 960 cm^{-1} is always present. The high-frequency range of the Raman spectrum is characterized by intense bands at 3272, 3446, and 3581 cm^{-1}, corresponding to ν_4, ν_3, and ν_1 OH-stretching bands in the FTIR spectra. These strong bands demonstrate an unusually high water content of 8.5%. There is also an unusually high Al and a moderate B content. At pressures around 9 GPa, the incorporation of water and Al in the weight-% level is not possible. Therefore, we assume a primary crystallization as ultra hydrous stishovite at very high pressure (~30 GPa) and a transformation of this stishovite into coesite during decompression during extremely rapid transport towards the surface. As a result of this process, the Al and OH initially incorporated into the stishovite passed over into a new lattice of the new coesite phase, probably in a metastable form. In this process, corundum-like groups are formed in the coesite lattice. Because of the significantly different Raman characteristics, we refer to this new phase as coesite-W – W for Waldheim, as we are unaware of any similar discovery, including synthetic analogues.

Kurzfassung

In diesem Beitrag untersuchen wir die sehr seltenen Coesit-ähnlichen Kristalle im Prismatin des Granulits von Waldheim/Sachsen mit der Raman-Spektroskopie. Dieser Coesite zeigt deutlich ein unterschiedliches Raman-Spektrum mit den charakteristischen Banden bei 272 und 339 cm^{-1} zusätzlich zu der starken Bande zwischen 521 und 528 cm^{-1}. Zusätzlich zu diesen Banden ist eine weitere starke Bande bei etwa 960 cm^{-1} immer anwesend. Der hochfrequente Bereich des Raman-Spektrums ist durch Intensitäts-starke Banden bei 3272, 3446 und 3581 cm^{-1} charakterisiert, diese entsprechen den ν_4, ν_3 und ν_1 OH-Stretch-Schwingungen in den FTIR Spektren. Diese starken Banden demonstrieren einen ungewöhnlich hohen Wassergehalt von 8,5%. Auch der hohe Al und der gemäßigte B Gehalt sind ungewöhnlich. Bei einem Druck von 9 GPa ist der Einbau von Wasser und Al im Prozent-Niveau nicht möglich. Deshalb nehmen wir für die Kristallisation des extrem H_2O-reichen Stishovites einen sehr hohen Druck (~ 30 GPa) an. Die Transformation des Stishovites in Coesite erfolgte während Dekompression beim extrem raschen Transport in Richtung zur Oberfläche. Infolge dieses Prozesses, wird das Al und auch OH vom Stishovit-Gitter von der neuen Coesite Phase, wahrscheinlich metastabil, übernommen. In diesem Prozess werden Korund-ähnliche Gruppen im Coesite Gitter gebildet. Wegen der doch signifikant unterschiedlichen Merkmale im Raman-Spektrum nennen wir diese neue Phase Coesite-W - W für Waldheim.

Keywords: Ultra-hydrous coesite, changing intensity ratios, blue shift, remnants of stishovite, Raman spectroscopy

Anschriften der Autoren
Dr. sc. nat. Rainer Thomas, Im Waldwinkel 8, D-14662 Friesack, Germany; e-mail: RainerThomas@t-online.de; ORCID 0000-0002-7699-7009
Paul Davidson, PhD, Codes, Centre for Ore Deposits and Earth Sciences, University of Tasmania, Hobart 7001, Australia; e-mail: paul.davidson@utas.au; ORCID 0000-0002-6128-0748
Dr. rer. nat. Adolf Rericha, Alemannenstraße 4a, D-14612 Falkensee, Germany; e-mail: ruth.rericha@gmx.de
Dipl.-Min. Ulrich Recknagel, Böhmerwaldstraße 22, D-86529 Schrobenhausen, Germany; e-mail: recknagel-sob@t-online.de

Fig. 1 Hand specimens a and b of the prismatine-bearing granulite from Waldheim/Saxony. All dark grains are prismatine crystals. Figure 1c is a detail of Figure 1b.

Abb. 1 Handstücke a) und b) des Prismatingranulits von Waldheim/Sachsen. Alle dunklen Körner sind Prismatinkristalle. Abbildung 1c ist ein Detail der Abbildung 1b.

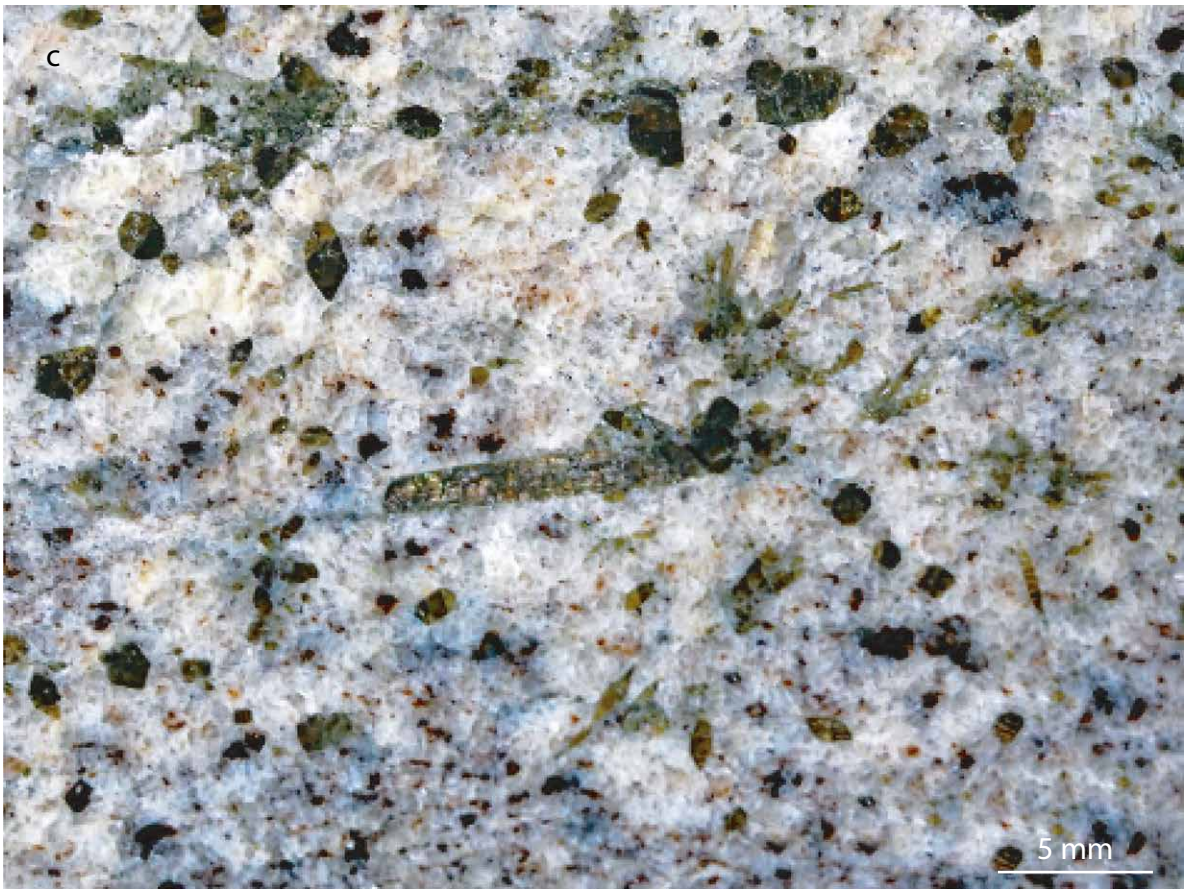

Introduction

The lens-shaped prismatine rock from Waldheim/Saxony forms a tiny body with a thickness of about 3 m and an extension of 15 m. The underlying bed is a quartz-rich granulite with sillimanite, and the hanging layer is composed of sillimanite and biotite.

Rötzler et al. (2008) and Hagen et al. (2008) give a detailed description of the rock (herein the sample number 163) and a detailed genetic interpretation and conclude that due to multi-stage overprinting, the prismatine granulite is unsuitable for determining peak P-T data.

However, a detailed Raman-spectroscopic study of the melt inclusions in pyrope, almandine, dravite, and prismatine and the mineral inclusions in the main minerals (prismatine, pyrope, almandine) give a very different picture. There is clear evidence in the occurrence of inclusions of the pressure indicator minerals stishovite and coesite in minerals from that sample that at least some of the prismatine rock has, in part, preserved a complex, high-pressure history. Other HP-HT-minerals observed here are diamond, moissanite, reidite, and HP-rutile, however, consideration of these phases will await later publication. The presence of numerous ultrahigh pressure minerals trapped as inclusions in lower pressure phases requires extremely rapid ascent from lower crustal depths to avoid inversion of the high-pressure minerals to low-pressure analogues (see Zagorsky 2007, Ni et al, 2017, Manning 2018). Thomas et al. (2022) have shown that the formation of stishovite and coesite is related to supercritical fluids coming very rapidly from great depth. These supercritical fluids or melts transport boron in addition to rounded micro-crystals (corundum, coesite-W and many others) for the pegmatite-like crystallization of prismatine, which enclose the spherical crystals without any reaction and recrystallization. This trapping prevents the recrystallization and transformation of the coesite-W into more stable polymorphs such as high-quartz and cristobalite.

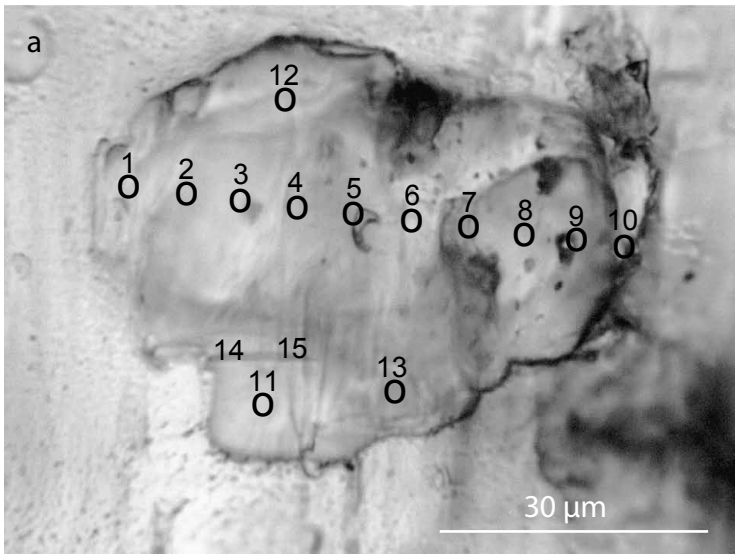

Fig. 2a Aggregate of coesite-I in prismatine from the Waldheim/Saxon Granulite Massif. Points 1–15 mark the points of the Raman measurements. Note that between the coesite and the prismatine, there is a partial thin layer of clinochlore.

Abb. 2a Coesit-I Aggregat im Prismatin von Waldheim im sächsischen Granulitgebirge. Die Punkte 1–15 markieren die Punkte der Raman-Messungen. Zwischen Coesit und Prismatin befindet sich teilweise eine dünne Klinochlor-Schicht.

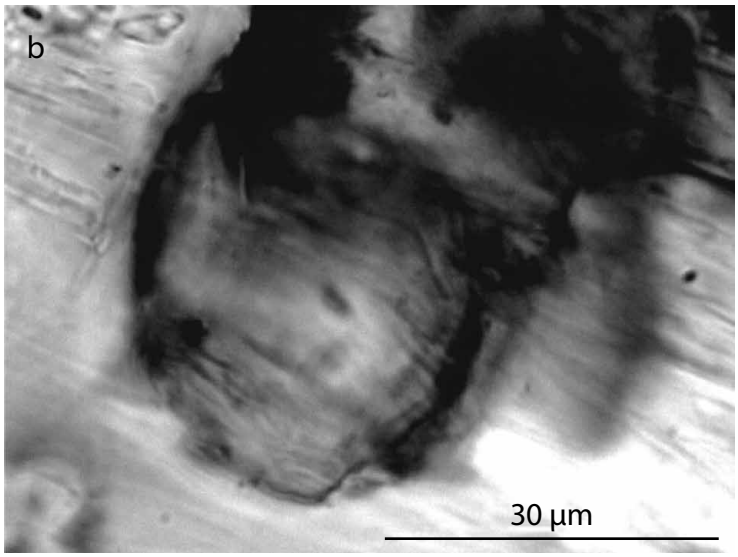

Fig. 2b The figure represents a larger elliptical coesite crystal (41 µm x 30 µm x 20 µm) in Fig. 2a around point 3.

Abb. 2b Die Abbildung zeigt einen großen elliptischen Coesit-Kristall (41 µm x 30 µm x 20 µm) in der Abbildung 2a, etwa am Punkt 3.

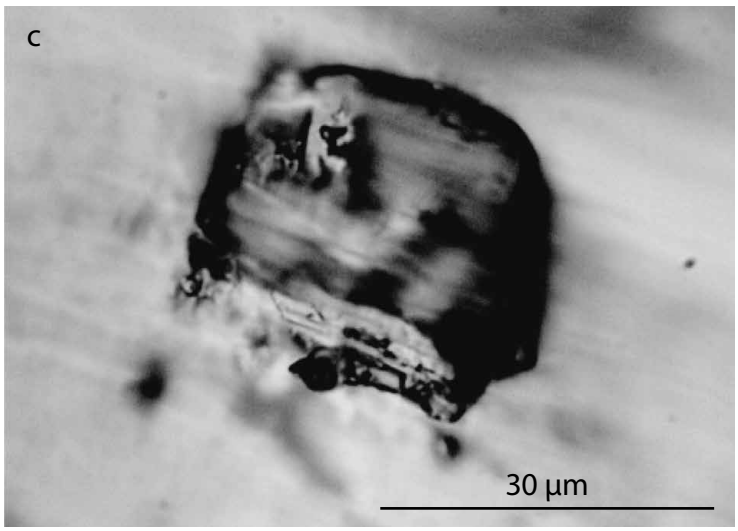

Fig. 2c Smaller coesite crystal (coesite-II).

Abb. 2c Kleinerer Coesit-Kristall (Coesit-II).

The trapped coesite-W is highly metastable as demonstrated during Raman measurements on a smaller crystal (coesite-II), from which only one Raman spectrum could be obtained. After the first measurement, this coesite could no longer be detected due to its inversion into stable quartz polymorphs and corundum.
Gigl & Dachille (1968) demonstrated that stishovite held at temperatures above 400 °C and up to 20 kbars converted completely into quartz in a few days. At slightly higher pressures, stishovite transforms completely to coesite. Thus Hemley et al. (1994) conclude that "no stishovite formed in the Earth's interior would be preserved over geological time in rocks at the surface." The same holds true for coesite, particularly for ultra-hydrous coesite. Coesite can only be found as inclusion in, for example, pyrope or clinopyroxene (Chopin 1984, Smith 1984, Kotkova et al. 2011), and diamond (Sobolev et al. 2000). The apparent stability of both minerals produced experimentally at high temperature and pressure at room-temperature is only indirectly related to the stability in the Earth's interior over geological time.
The purpose of the present paper is the description of unusual coesite (coesite-W) as inclusions in a prismatine crystal. In contrast to the previously described coesite crystals showing the very strong main line at 520 cm^{-1}, the coesite from Waldheim is characterized by four strong lines: 273, 339, 520-528, and 965 cm^{-1} with changing intensity ratios in relation to the 520 cm-1 band, independent of the crystallographic orientation. Other characteristic feature is the intense OH-stretching bands beyond 2500 cm^{-1}.

Methods and sample

Method

The Raman method, particularly the polarization-orientation (P/O) micro-Raman spectroscopy, is complementary to micro-X-ray diffraction and should be used when X-ray analysis is not practical or possible. It is worth noting that the Raman polarizability tensor is fixed relative to the position of the atoms and the directions of the chemical bonds between them (Tuschel 2020). However, given the metastability of the Waldheim coesite and the position in the prismatine host, a complete set of the necessary Raman spectra cannot be obtained. Furthermore, other methods (X-ray, TEM) cannot be considered due to the high probability of destruction of these rare samples.
Raman spectra were recorded with the EnSpectr Raman microscope RamMics M532 in the spectral range of 80–4000 cm^{-1} using a 50 mW single mode 532 nm laser, an entrance aperture of 20 µm, a holographic grating of 1800 g/mm, and a spectral resolution of 4–6 cm^{-1}. Depending on the grain size, we used microscope objectives with magnifications between 3.2x and 100x. As 100x lens, we used the long-distance LMPLFLN100x from Olympus. The laser energy on the sample can continuously be adjusted down to 0.02 mW. The position of the Raman bands was controlled before and at the end of each series of measurements of the Si band using a single crystal chip of semiconductor-grade silicon. The run-to-run repeatability of the line position (from 20 measurements each) was ± 0.3 cm^{-1} for Si (520.4 ± 0.3 cm^{-1}) and 0.5 cm^{-1} for diamond (1332.3 ± 0.5 cm^{-1} over the range 80 – 2000 cm^{-1}), respectively. As diamond reference we used a water-clear natural diamond crystal.
Some test and control measurements were performed with the 405 nm laser of the Jobin-Yvon LabRam HR800 spectrometer (grating 1800 g/mm) at the GFZ Potsdam.
We used an Olympus rotating microscope stage to determine the azimuth-dependent Raman intensity.
For identifying diamond and moissanite as inclusions in minerals of the prismatine rock, we applied only fresh samples which were never handled with diamond saws and/or with diamond- and SiC-bearing grinding and polishing materials (see Keller and Ague, 2022).
For identifying the different mineral phases using Raman micro-spectroscopy, we used the RRUFF database (Lafuente et al. 2015), as well as the data given in Hurai et al. 2015 and our own reference material.
The Al content of the Waldheim coesite was estimated using the 415.6 ± 0.9 (n = 10) corundum line in coesite. As references, we used a Silicon-on-Sapphire (SOS) crystal and a single crystal of leucosaphire with the 417.2 ± 0.8 cm^{-1} band (n = 10 measurements).
The water content was determined using three Raman bands (3274, 3448 and 3567 cm^{-1}) in the high-frequency range. As reference we used the synthetic coesite sample MKM-00-15 with 200 ppm H_2O (see Koch-Müller et al. 2001). A second method described by Thomas (2000), Thomas et al. (2006 and 2009) was also used. In this, we used an albite glass with 10,0 % H_2O, cross-checked with 30 different glasses of well-characterized water concentration.

We would emphasize that with the micro-Raman spectroscopy techniques used, the following principle information can be obtained:

a) The characteristic Raman frequencies give clear evidence as to the mineral phase in question (Hurai et al. 2015. Lafuente et al., 2015)
b) The frequency shift of some bands relates to strain and atomic substitution (Tuschel, 2017, Fluegel et al. 2015).
c) The intensity of the Raman bands gives, among other things. Information on the quantitative amount of some species dissolved in the host (e.g., Thomas 2000).
d) The polarization dependency of the Raman intensity gives information on the crystal orientation (Tuschel, 2012).
e) The linewidth gives information regarding microstrain and amorphization (Tuschel 2017).

Sample

During the inspection of minerals from the famous prismatine rock from Waldheim/Saxony (Waldheim station) (Fig. 1), Thomas and Grew (2021) found two coesite aggregates composed of small ellipsoidal coesite crystals in the same growth zone of a prismatine crystal. Both coesite aggregates have a dimension of 64 x 45 µm (coesite-I) and 30 x 25 µm (coesite-II), respectively (Fig. 2). A larger spherical crystal aggregate has a diameter of 32 µm and is up to 20 µm thick. Both coesite crystals lie at the surface, and they are partially covered with a very thin layer of prismatine. A thin clinochlore layer is partly under the crystal aggregates. Both coesites show no inversion to quartz. The often-described radial cracking of the host mineral, here prismatine, around the inclusions is completely missing, showing that the elliptical coesite grains were integrated during the prismatine growth. However, radial cracking only demonstrates that there has been an expansion of the inclusion post-trapping. Its absence only indicates similar coefficients of expansion of the host and the inclusion.

Given the rarity and geometric position of the coesites in prismatine from Waldheim and the destructive nature of microprobe, TEM and X-ray studies (as a result of the metastability problem), these techniques should be performed only as a final step, which at the moment we exclude to preserve these samples.

For the genetic interpretation, it is essential to observe that in almost every mineral of the prismatine granulite rock in our sample, there are spherical-subspherical mineral grains with diameters between 10 to 50 µm. Euhedral inclusions are rare. The surfaces of these grains are usually extremely smooth – Kalkowsky (1907) described them as smooth, like oil drops. We estimate the frequency of these grains at 180 spheres/cm^3 in the whole rock.

The following spherical, elliptical or subspherical crystals could be identified: zircon, zircon-reidite, dravite, garnet, quartz, rutile, corundum, kyanite feldspars, molybdenite, moissanite, diamond. Also, the rare coesite forms round spherical aggregates in prismatine composed of some smaller spherical coesite crystals. All such spherical crystals are entirely out of place with respect to the Waldheim prismatine – they are foreign bodies. There are non-equilibrium signs such as the absence of any equilibrium faces and show none of the post-entrapment shape modification as described by Cesare et al. (2021)

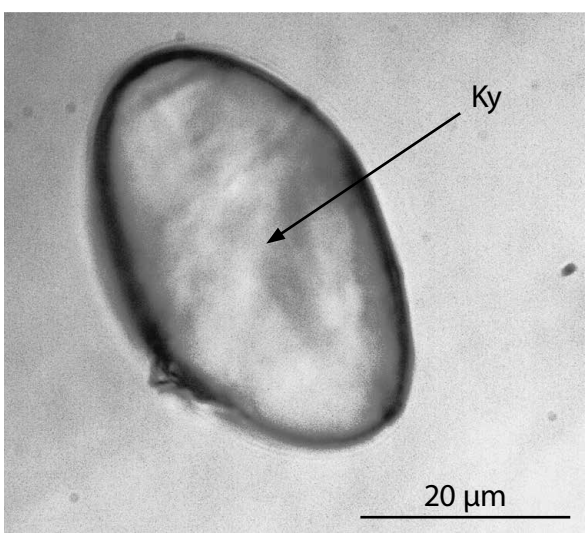

Figure 3 shows an elliptical kyanite crystal in prismatine from Waldheim. Similar elliptical crystals are shown in Thomas et al. (2022).

In prismatine rock, such spherical crystals are not common; however, once recognized, they are quite distinctive. Moreover, these are not only found in the prismatine rock. Such crystals we have also found in the mafic

Fig. 3 Elliptical kyanite inclusion in dravite. Not far from this inclusion is a spherical aggregate of nano-diamond, moissanite and graphite, as well as supercritical melt inclusion (Fig. 9 in Thomas et al. 2022).

Abb. 3 Ein elliptischer Disthen-Einschluss im Dravit. In der Nähe befindet sich ein sphärisches Aggregat bestehend aus nano-Diamant, Moissanit und Graphit, sowie ein superkritischer Schmelzeinschluss (Fig. 9 in Thomas et al. 2022).

granulite from Tirschheim (SW end of the Granulite Massif, about 41 km from the Waldheim location) and also in abyssal (metamorphic) pegmatites related to anatectic processes in high-grade metamorphic rocks of upper amphibolite to granulite facies of the Starkoč pegmatite in the Gföhl unit, Bohemian Massif (see Novák & Cempírek 2010).

Results

Coesite in prismatine from Waldheim

Figure 4 shows the differences in the Raman spectra between the synthetic coesite MKM-00-15 (upper spectrum) and the natural coesite from Waldheim (lower spectrum). Conspicuous in the Waldheim coesite are strong OH-bands in the high-frequency range beyond 2500 cm^{-1}. The band at 2660 cm^{-1} is associated with AlOH defects, and the bands at 2822, 2961, 3097, and 3751 cm^{-1} with BOH defects. The band also indicates boron in the Waldheim coesite at 639 cm^{-1}, which is clearly attributed to the formation of a borosilicate structure (Manara et al. 2009) and our own measurements on reedmergnerite-based glasses. The weak band at 589 ± 0.3 cm^{-1} corresponds to the most intense Raman line of reedmergnerite (Manara et al. 2009). Note, the feldspar reedmergnerite [$NaBSi_3O_8$] - the boron analog of albite, according to cell data fits very well with the coesite structure (see also Tschauner, 2019).

Table 1 provides the Raman bands of the Waldheim coesite (mean of the profile shown in Fig. 2a) compared to a synthetic coesite crystal MKM-00-15 (Koch-Müller et al. 2001) and the data given by Hemley (1987).

Although there are certain similarities between the synthetic and the natural coesite from Waldheim, there is also a very significant difference. The Waldheim coesite is characterized by three strong bands at 272, 339, and 527 cm^{-1}. The 339 cm^{-1} band is generally the most substantial band in the Raman spectrum. The interdependence of the intensity between the 520 and 332 cm^{-1} bands during rotation around the sample normal is conspicuous. Furthermore, in nearly all Raman spectra of coesite, we see remnants of stishovite, indicated by pressure or composition shifted Raman bands at (B_{2g}) 952.3 ± 4.8, (A_{1g}) 770.9 ± 4.4, (E_g) 582.9 ± 5.0, (B_{1g}) 206.9 ± 5.2 cm^{-1}. Some Raman coesite spectra still show remnants of the strong stishovite bands at about 2940 cm^{-1}.

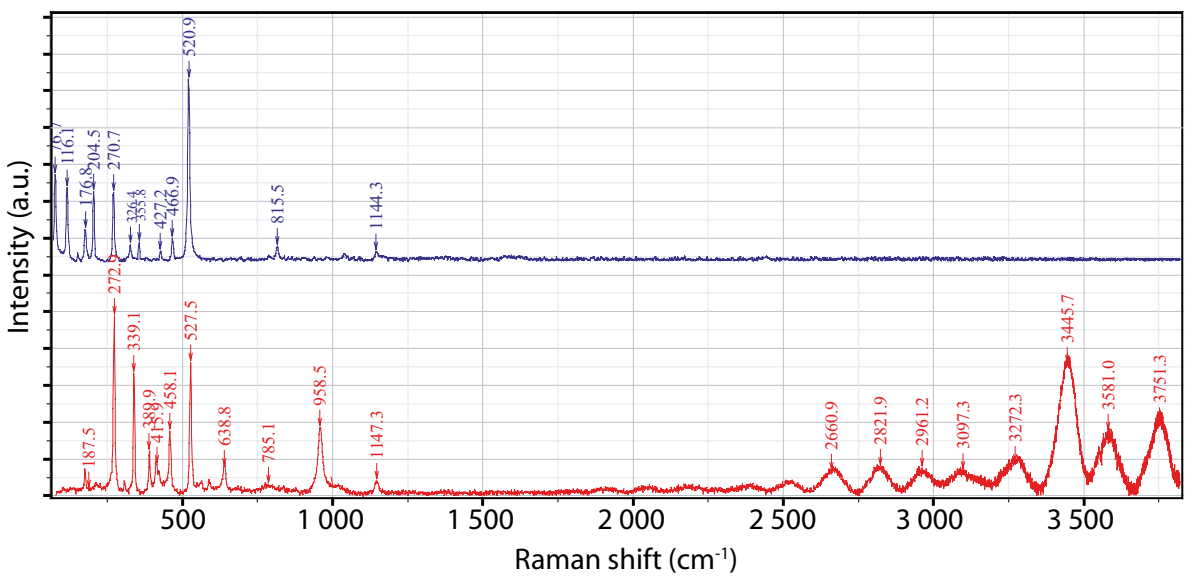

Fig. 4 Raman spectra of synthetic coesite (upper spectrum) and the natural Waldheim coesite (lower spectrum). The OH-band in the high-frequency range demonstrates the high-water content in the Waldheim coesite. The MKM-00-15 coesite contains only 200 ± 25 ppm H_2O (Koch-Müller et al. 2001).

Abb. 4 Das obere Spektrum zeigt das Raman-Spektrum eines synthetischen Coesites, und im unteren Spektrum ist der natürliche Coesit von Waldheim dargestellt. Die OH-Banden im Hochfrequenzbereich weisen auf den hohen Wassergehalt im Waldheimer Coesit hin. Der MKM-00.15 Coesit enthält nur 200 ± 25 ppm H_2O (Koch-Müller et al. 2001).

According to Hemley (1987), the optical vibrations of coesite are described by Γ_{op} = 16 A_g + 17 B_g + 18 A_u + 18 B_u, where A_g and B_g species are Raman-active, and the A_u and B_u species are infrared-active. From the 33 predicted A_g and B_g vibrations, only 20 bands were observed, and 18 Raman-active vibrations are tabulated by Hemley (1987). The coesite from Waldheim shows some strong Raman-active bands, which are not predicted. These include the always present bands at about 960 and the extreme band between 330 and 340 cm^{-1}. Furthermore, some bands indicate a vigorous orientation-dependent intensity, atypical for all studied synthetic coesites. Figure 4 is an example of this observation.

In most of the coesite crystal literature, the 520 cm^{-1} band is the prominent and strongest Raman band. The widespread presence of a band at 959 cm^{-1} (for simplification 960 cm^{-1} band), which is missing in most previously described coesite, is conspicuous in the Waldheim coesite. Only synthetic coesite, grown in the stishovite field, show this band - however it is not so strong. We interpret this band as isolated SiO_4 tetrahedra [$\nu_3(T_2)$] generated by the transition of stishovite into coesite.

In some cases, there is a peculiar and significant shift of the 520 cm^{-1} bands to about 527.5 cm^{-1}. Such a shift is interpreted by, for example, Korsakov et al. (2020) as residual pressure within the inclusions. This interpretation for the coesite in prismatine described herein is inconsistent because the crystal aggregates lie almost free on the sample surface – only covered by a micrometre thick prismatine layer and the consistent absence of radial cracking around these and other inclusions in the sample. However, we can interpret this shift as resulting from the "frozen" pressure at trapping conditions produced by a significant insertion of Al, B, and OH, which is only possible at a significantly higher pressure such as 8.6 GPa at 1000°C (Ono et al. 2017) see also Nisr et al. (2017). That Al is an important component of the coesite-W lattice can be seen from the correlation of the corundum-typical band with all other prominent coesite bands shown in Fig. 5. From the intensity of the 414 cm^{-1} line in the coesite, which corresponds to the strongest band of corundum, we estimate an Al content of 3.2 ± 1.6 %.

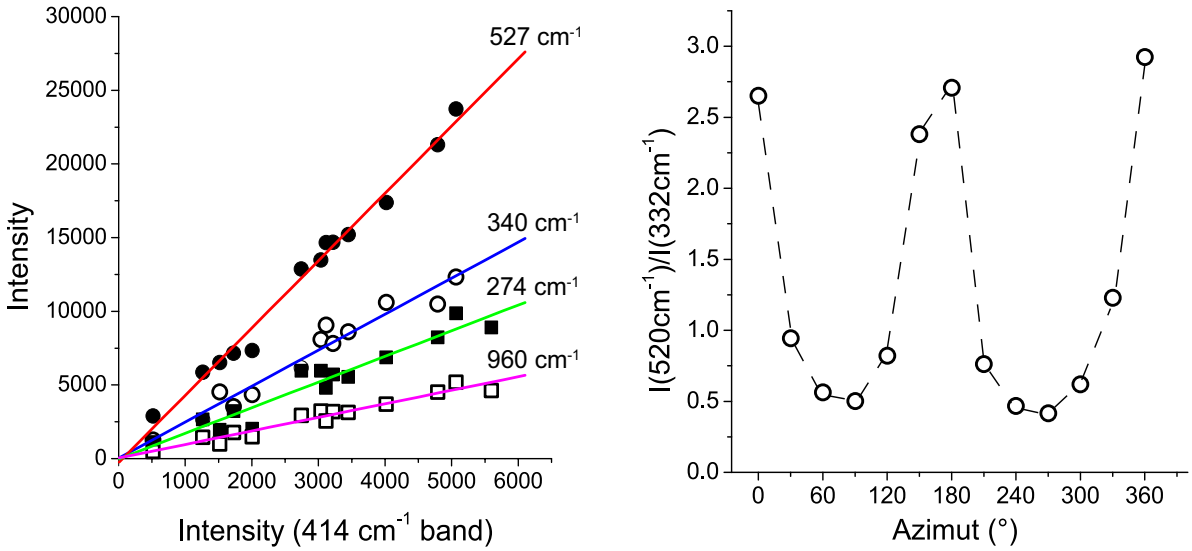

Fig. 5 Correlation of the intensity of some coesite-I bands against the intensity of the 414 cm^{-1} band, which is representative of corundum (417.2 ± 0.8 cm^{-1}) in the sample.

Abb. 5 Korrelation der Intensität einiger Coesit-I Banden mit der Intensität der 414 cm^{-1}-Bande, die dem gelöstem Korund (417.2 ± 0.8 cm^{-1}) in der Probe entspricht.

Fig. 6 The intensity ratio of the coesite main band at about 520 cm^{-1} versus the new and dominant 332 cm^{-1} band is independent of the polarization and orientation of the sample (azimuth). Note, that this method is a type of the very sensitive polarization/orientation (P/O) micro-Raman spectroscopy (see Tuschel 2020) and shows further that the 332 cm^{-1} band of the coesite from Waldheim is clearly a component of the coesite-W lattice.

Abb. 6 Das Intensitäts-Verhältnis zwischen der 520 cm^{-1} Coesit-Bande und der neuen und dominanten 332 cm^{-1}-Bande in Abhängigkeit von der Polarisation und Orientierung (Azimut) der Probe. Zu bemerken ist, dass diese Methode eine sehr empfindliche Polarisation/Orientierung (P/O) der Mikro-Raman-Spektroskopie ist. Weiterhin wird klar gezeigt, dass die 332 cm^{-1}-Bande des Coesits von Waldheim eine Komponente des Coesit-W-Gitters ist.

The intensity ratios between the 273, 339, and 520 cm^{-1} bands vary enormously with the orientation of the studied coesite, and here the ratio between the 339 and the 520 cm^{-1} bands shows the largest variations. Figure 6 shows the relationship between the intensity ratio between the 520 and the new 332 cm^{-1} bands with the azimuth. From this figure, it follows that the intensity ratio is strongly dependent on the crystallographic orientation and varies between 3 and 0.5. Synthetic coesite shows similar behaviour for the 520/265 cm^{-1} intensity ratio and the azimuth, however, the ratio differs only between 3 and 2. The intensity of all strong Raman bands of the Waldheim coesite show a very well linear correlation with each other (Fig. 5). In contrast, a Raman band from an extraneous mineral (e.g., from the background) gives no correlation with any coesite band.

Unusual Raman spectra of the Waldheim coesite

Table 1 clearly shows the differences between both coesite types. In the Raman spectrum of the coesite from Waldheim, there are fewer bands, and three of these show variable, extreme intensities. Figure 7a provides the Raman spectra of the synthetic coesite MKM-00-15 (blue) and the coesite from Waldheim (red). In part,the difference is huge.

Figure 7b shows two typical Raman spectra of the Waldheim coesite with a different orientation at the same point (0 and 90°). Indicated are the small Raman bands, which show Al^{3+} and BO_4^- portions in the coesite lattice.

All these observations imply chemically different coesite with changed crystallography and symmetry. According to Tuschel (2017), dopants or impurities at low concentrations (<1%) do not affect the lattice vibration modes of the host crystal. However, at levels greater than 1%, shifting and broadening of some Raman bands are generated. The significantly different spectra (Tab. 1) and the always present bands for corundum, especially the doublet at 414-422 cm^{-1}, is strong evidence that the original Al content of the coesite was significantly greater than 1 %. The same is true for B (see Manara et al. 2009). That can be demonstrated by the good correlation between the intensities of the new 339 cm^{-1} coesite band and the 414 cm^{-1} band of corundum shown in Fig. 6., and maybe the bands at 641 cm^{-1} for boron. Similar correlations also occur with other coesite bands. Thus demonstrating that practically all of the crucial bands are part of the coesite and are not generated by other minerals. That is also true for the strong 960 cm^{-1} band.

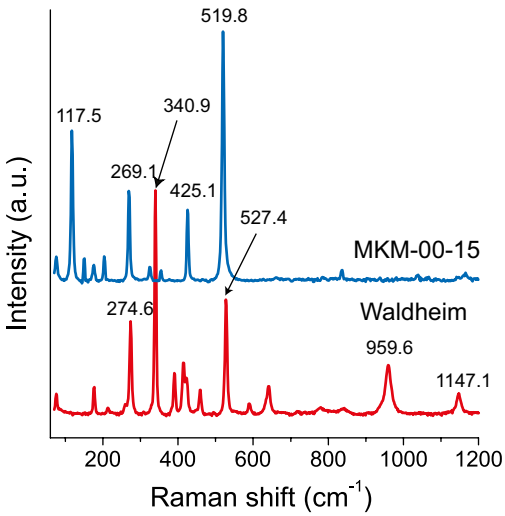

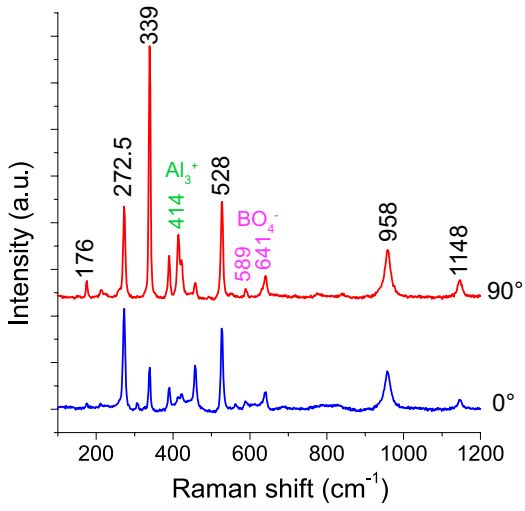

Fig. 7a Raman spectra of synthetic coesite (MKM-00-15) compared to the Waldheim coesite-I.

Abb. 7a Das Raman-Spektrum des synthetischen Coesits (MKM-00-15) im Vergleich zum Coesit-I von Waldheim.

Fig. 7b Two typical Raman spectra of the Waldheim coesite with a different orientation at the same point (0 and 90°). Indicated are the small Raman bands, which show Al^{3+} and BO_4^- portions in the coesite lattice.

Abb. 7b Zwei typische Raman-Spektren des Coesits von Waldheim bei unterschiedlichen Orientierungen (0 und 90°) am gleichen Meßpunkt. Gezeigt werden die schwachen Raman-Banden, die die Al^{3+}-und BO_4^--Anteile im Coesit-Gitter andeuten.

Table 1 Raman bands of coesite inclusions (coesite-I and coesite-II) in prismatine from Waldheim in comparison to data obtained from a synthetic coesite crystal MKM-00-15 (Koch-Müller et al. (2001) [532 nm, 28 mW on sample]) and the reference data from Hemley (1987).

Tabelle 1 Raman-Banden der Coesit-Einschlüsse (Coesit-I und Coesit-II) im Prismatin von Waldheim im Vergleich zu Daten, die von einem synthetischen Coesit-Kristall MKM-00-15 (Koch-Müller et al. (2001) {532 nm, 28 mW auf der Probe) und den Referenz-Daten von Hemley (1987) stammen.

Coesite-I in prismatine/ Waldheim	Coesite-I (405 nm)	Coesite-II in prismatine/Waldheim	Coesite MKM-00-15	Coesite (Hemley 1987)
75.7 ± 2.1 w	n.d.	75.0 w	75 m	77 s
			115 s	116 s
			148 m	151 m
176.0 ± 0.6 w	178.7 vw		175 m	176 s
			202 m	204 m
212.6 ± 1.7 m	213.8 vw			
272.2 ± 2.0 s	274.3 vs	273.3 vs	268 s	269 s
			323 w	326 m
338.8 ± 1.4 vs	340.4 s	339.7 m		
			352 w	355 m
422.4 ± 1.2 w	414.8 w	415.0 w	424 w	427 m
455.8 ± 3.8 w	459,5 s	459.4 s	464 w	466 m
527.0 ±1.3 vs	528.9 vs	528,6 vs	519 vs	521 vs
590.2 ± 0.6 w	590.4 w	589.3 w		
640.3 ± 0.6 w		641.9 m		
				661 w
779.0 ± 3.7 w	791.2 w	792.1 w	782 vw	795 w
			814 vw	815 w
958.8 ± 1.6 m to s	960.3 s	960.4 s		
			1037 vw	1036 w
				1065 w
1147.3 ± 2.5 m	1146.6 vw	1147.4 vw	1143 vw	1144 w
				1164 w

Relative intensity of the Raman bands: vw – very weak, w – weak, m – medium, s – strong, vs – very strong: n. d. – not detected, because the entry of the 405 nm laser starts at 100 $cm^{-1.}$

The anomalous behaviour of the Waldheim coesite

In the Waldheim coesite, a further anomaly was observed – the significant blue shift of most Raman bands dependent on the laser intensity (Figure 8). The origin of this shift is found in the crystal structure or the relationship of the heteroepitaxial intergrowth between prismatine and coesite. Typical of the Waldheim coesite is the very intense Raman band at 339 cm^{-1}, which can

a) be traced back to a classical, frozen pressure shift of the weak 326 cm^{-1} standard bands by the pressure of 13.4 GPa, by the
b) change of the lattice parameters by incorporation of Al and H_2O by a coupled substitution ($Si^{4+} = Al^{3+} + H^{+}$), or
c) by deformity of coesite with the substrate, in part prismatine and clinochlore, and
d) by lattice mismatch produced by the transformation of stishovite into coesite. In the Raman spectrum taken parallel to the c-axis, this line (339 cm^{-1}) is very strong and stronger than the 520–528.5 cm^{-1} lines.

This apparent anomaly needs an explanation. A metastable conservation of a former pressure state is only possible if the crystals in question are entirely encapsulated in a stable mineral like garnet or diamond. To the second point (b): A first estimation of the water concentration (using the 3403.4 cm^{-1} bands) for the Waldheim coesite

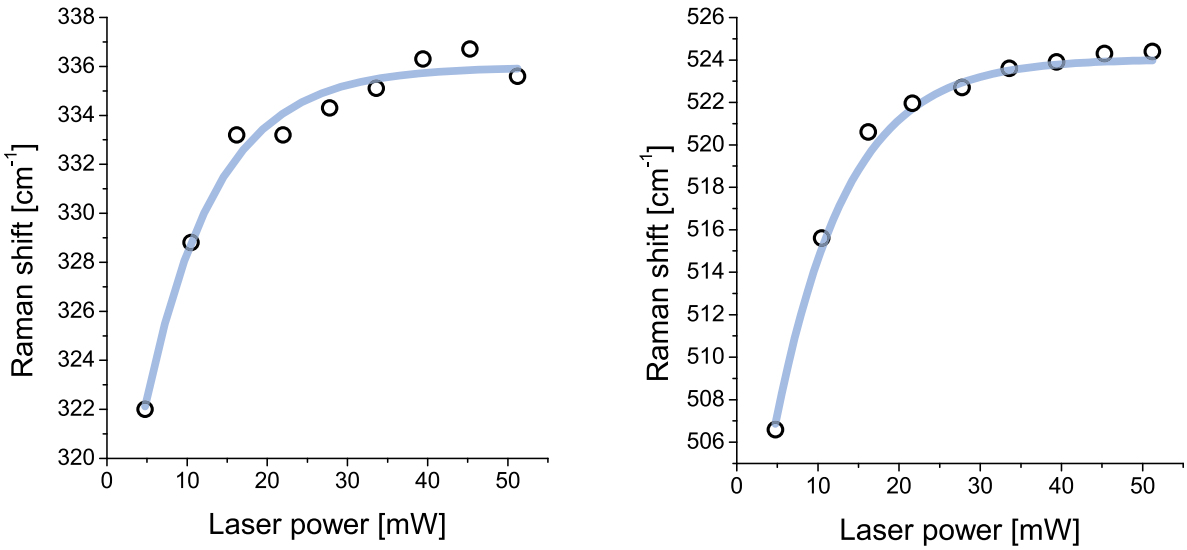

Fig. 8 The Boltzmann sigmoidal fit of the blue shift of prominent coesite bands at 330 and 520 cm^{-1} is independent of the laser excitation (532 nm). The significant blue shift (~18 cm^{-1}) results from the strain generated by the lattice mismatch between primary stishovite (now only remnants) and the resulting coesite. The amount of the blue shift is only quasi-reversible because the blue shift declines with time signalling the destruction of the metastable coesite lattice. Note that no synthetic coesite, stishovite, or mixing of both mineral phases shows such a blue shift.

Abb. 8 Boltzmann-Sigmoidfunktionsanpassung der Blau-Verschiebung der prominenten Coesit-Banden bei 330 und 520 cm^{-1} in Abhängigkeit von der Laser-Leistung (für 532 nm). Die deutliche Blau-Verschiebung (~18cm^{-1}) resultiert aus der Spannung, die durch Gitterabweichungen zwischen dem primären Stishovit (jetzt nur noch Reste) und dem gebildeten Coesit. Der Betrag der Blau-Verschiebung ist nur quasi-reversibel, weil die Blauverschiebung mit der Zeit abnimmt, da das Coesit-Gitter metastabil ist. Wichtig ist, dass synthetischer Coesit, Stishovit oder Mischungen beider Minerale keine Blauverschiebung zeigen.

gives 1.02 (%(g/g)) and up to now is the highest water concentration for natural coesite. However, this high-water content must also be considered in the context of the fourth case (d). Note, however, that this value for the water content was obtained from thin coesite crystals (point 6-15). By the repeated measurements on these points, a loss of water during measurement is highly possible (see Frigo et al. 2019 and Thomas et al. 2022).

To see if the observed strong blue shift comes from the Raman spectrometer, we have performed Raman measurements on an ideal SOS sample (Silicon on Sapphire). This sample is characterized by an epitaxial Si layer on a single crystal wafer of sapphire. We have taken Raman spectra of Si at different laser power from 10 to 100% of the 532 nm laser – 100% correspond to 50 mW. For the Si main line result, a value of 520.1 ± 1.8 cm^{-1}. That means that the spectrometer and the used laser power do not generate the large blue shift in the coesite spectra. Furthermore, indicating that the device is not defective. A synthetic single coesite crystal (MKM-0015) gives a value of 518 ± 1.6 cm^{-1} for the 520 cm^{-1} band and no blue shift.

For the large blue shift for the Waldheim coesite, there are the following possibilities:

- strain produced by the heteroepitaxial relationship of a thin coesite layer on clinochlore
- lattice mismatch produced by the transformation of stishovite into coesite, and
- cationic substitution because the coesite's water content is unusually high.

According to Tschauner (2019), stishovite can accommodate Al and H_2O through coupled substitution at a pressure above 30 GPa. At lower pressure, the substitution is only beyond the trace element level. The possible higher content of Al and OH is, therefore, evidence of significantly higher trapping pressures. By transforming stishovite into coesite, the originally incorporated Al and OH pass over, possibly in a metastable form, into the new lattice. In this process, corundum is formed in the coesite lattice (possibly as a type of point defect). As a first approximation, we obtained a minimum Al content in the Waldheim coesite of 3.2 ± 1.6 % Al. Minimum, because the Raman intensity depends on the orientation of the sapphire wafer. We used the maximal intensity values of the sapphire wafer reference (otherwise, higher Al-concentrations would result).

Water in coesite was determined using the Raman bands at 3274, 3448 and 3567 cm^{-1}, in analogy to the FTIR spectroscopy (Koch-Müller et al. (2003). A value of 7925 ppm H_2O was obtained. Using the technique described by Thomas et al. (2009) and using a silicate glass with 5.01 % water, 11750 ppm H_2O results. These values were obtained only from thin coesite parts outside the 20 µm thick spherical crystal (points 6-15 in Fig. 2a). Using the spherical coesite crystal, the Raman measurement yield as mean 8.5 ± 1.3 % H_2O_t (12 determinations using the albite glass with 10.0 % H_2O). For the determination, we used only the strong band at 3448 cm^{-1}, because the 3567 cm^{-1} band is, in part, affected by the OH-band of prismatine with bulk water of 3.6 ± 0.6 % H_2O. Such high values for water have previously never been found in natural coesite. This is maybe due to the faster transformation of water-rich coesite back to quartz (see Frigo et al. 2019). Note, however, that the stishovite found in the same rock (Thomas et al. 2022) also contains 8.5% H_2O, underlining the primary origin of the coesite from ultra-hydrous stishovite. Figure 9 gives some details of the Raman spectra of the Waldheim coesite, belonging to the coesite spectrum in Fig. 7b (90° position) in relation to the H_2O-reference (10,0 % H_2O).

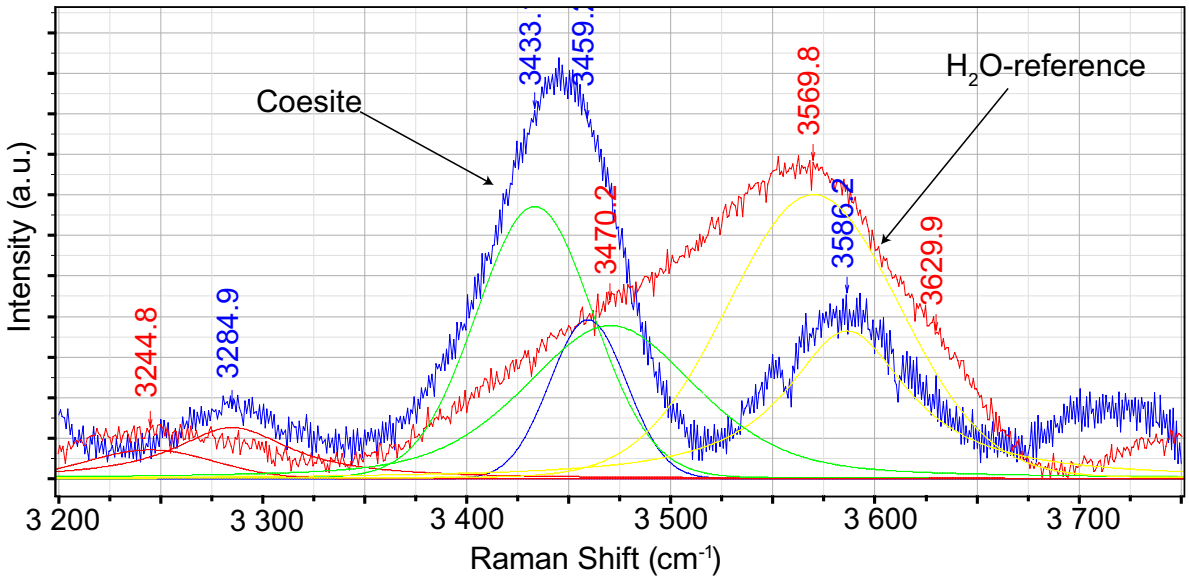

Fig. 9 Estimation of the water content of the Waldheim coesite**:** Raman spectrum of coesite (blue) in comparison to the H_2O-reference (10.0 % H_2O).

Abb. 9 Abschätzung des Wasser-Gehaltes des Waldheim Coesites: Raman-Spektrum des Coesit (blau) in Vergleich zum H_2O-Standard (10.0% H_2O).

Conclusions

Prismatine from Waldheim encloses scarce coesite crystals that differ significantly from all previously described coesite crystals, natural or synthetic. The appearance of three strong Raman bands, which are not predicted by the factor group analysis (Hemley 1987) makes it plausible that the coesite from Waldheim is strongly different to all natural and synthetic coesites, and is possibly an Al-, B- and water-rich metastable coesite with a different symmetry. The reduced number of valid Raman lines supports the presumption of the changed symmetry. We call this mineral phase as coesite-W; W is standing for Waldheim.

Tuschel (2019) wrote: "If the complete set of peak positions of a sample spectrum does not match any of those of your reference spectra, you may have discovered a new polymorph."

The high water content of the coesite and its predecessor stishovite phase have a great potential for incorporating weight per cent levels of H_2O in the crystal structure and has also the potential to be a pivotal phase for transporting and storing water in the lower mantle (Lin et al. 2020). Furthermore, our observation demonstrates that supercritical melt/fluid phases can, in addition to the volatile components, also transport solid mineral pha-

ses very rapidly from the mantle to the crust. Further that also may imply significant amounts of heat energy may also be transported into the upper crust. The influence such energy and matter flow has on the redistribution of element remains an interesting conjecture.

Acknowledgements

We thank Dr Ilias Efthimiopoulos (GFZ Potsdam) for the discussion of the blue shift, Prof. Dr Monika Koch-Müller for synthetic coesite and stishovite crystals and the H_2O coesite reference. The manuscript benefited from long-lasting discussions with Edward Grew. Prof. Dr Ronny Roessler is thanked for his editorial handling of the manuscript.

References

Cesare, B.: Parisatto, M.; Mancini, L.; Peruzzo, L.; Franceschi, M.; Tacchetto, T.; Reddy, S.; Spiess, R.; Nestola, F. & Marone, F. (2021): Mineral inclusions are not immutable: Evidence of post-entrapment thermally-induced shape change of quartz in garnet. – Earth Planet. Sci. Lett., **555**: 116708, 1–11.

Chopin, C. (1984): Coesite and pure pyrope in high-grade blueschists of the Western Alps: a first record and some consequences. – Contrib. Mineral. Petr., **86**: 107–118.

Fluegel, B.; Mialitsin, A. V.; Beaton, D. A.; Reno, J. L. & Mascarenhas, A. (2015): Electronic Raman scattering as an ultrasensitive probe of strain effects in semiconductors. – Nature Communications, **6**: 7136, 1–5

Frigo, C.; Stalder, R. & Ludwig, T. (2019): OH defects in coesite and stishovite during ultrahigh-pressure metamorphism of continental crust. – Phys. Chem. Miner., **46**: 77–89.

Gigl, P. D. & Dachille, F. (1968): Effect of Pressure and Temperature on the Reversal Transitions of Stishovite. – Meteoritics, **4**: 123–136. https://doi.org/10.1111/j.1945-5100.1968.tb00379.x

Hagen, B.; Hoernes, S. & Rötzler, J. (2008): Geothermometry of the ultrahigh-temperature Saxon granulites revised. Part II. Thermal peak conditions and cooling rates inferred from oxygen-isotope fractionation. – Eur. J. Mineral., **20**: 1117–1133.

Hemley, R. J. (1987): Pressure dependence of Raman spectra of SiO_2 polymorphs: α-quartz, coesite, and stishovite. – In: Manghnani, M. H. & Syono, Y (eds.): High-Pressure Research in Mineral Physics. pp. 347–359.

Hemley, R. J.; Prewitt, C. T. & Kingma, K. J. (1994): Chapter: High-pressure behavior of silica. – Silica, **29**: 41–82. https://doi.org/10.1515/9781501509698-007

Hurai, V.; Huraiova, M.; Slobodnik, M. & Thomas, R. (2015): Geofluids – Developments in Microthermometr, Spectroscopy, Thermodynamics, and Stable Isotopes. Elsevier, 489 pp.

Kalkowsky, E. (1907): Der Korundgranulit von Waldheim in Sachsen. – Abhandlungen der Naturwissenschaftlichen Gesellschaft ISIS Dresden. S. 47–65.

Keller, D. S. & Ague, J. J. (2022): Possibilities for misidentification of natural diamond and coesite in metamorphic rocks. – N. Jb. Miner. Abh., **197**/3: 253–261.

Koch-Müller, M.; Fei, Y.; Hauri, E. & Liu, Z. (2001): Location and quantitative analysis of OH in coesite. – Phys. Chem. Miner., **28**: 693–705.

Koch-Müller, M.; Dera, P.; Fei, Y.; Reno, B.; Sobolev, N.; Hauri, E. & Wysoczanski, R. (2003): OH^- in synthetic and natural coesite. – Am. Mineral., **88**: 1436–1445.

Korsakov, A.V.; Kohn, M. J. & Perraki, M. (2020): Applications of Raman spectroscopy in metamorphic petrology and tectonics. – Elements, **16**: 105–110.

Kotkova, J.; O'Brien, P. J. & Ziemann, M. A. (2011): Diamond and coesite discovered in Saxony-type granulite: Solution to the Variscan garnet peridotite enigma. – Geology, **39**: 667–670.

Lafuente, B.; Downs, R. T.; Yang, H. & Stone, N. (2015): The power of database: the RRUFF project. – In: Armbruster, T. & Danisi, R. M. (eds.): Highlights in mineralogical crystallography. Berlin (W. De Gruyter), pp. 1–30.

Lin, Y.; Hu, Q.; Meng, Y.; Walter, M. & Mao, H. (2020): Evidence for the stability of ultrahydrous stishovite in Earth's lower mantle. – Proc. Natl. Acad. Sci. U.S.A., **117**: 184–189.

Manara, D.; Grandjean, A. & Neuville, D. R. (2009): Advances in understanding the structure of borosilicate glasses: A Raman spectroscopy study. – Am. Mineral. **94**: 777–784.

Manning, C. E. (2018): The Influence of Pressure on the Properties and Origins of Hydrous Silicate Liquids in Earth's

Interior. I – In: Kono, Y. & Sanloup, C. (eds.): Magmas Under Pressure – Advances in High-Pressure Experiments on Structure and Properties of Melts. Chapter pp. 83–113.

Ni, H.; Zhang, L.; Xiong, X.; Mao, Z. & Wang, J. (2017): Supercritical fluids at subduction zones: Evidence, formation condition, and physicochemical properties. – Earth-Sci. Rev., **167**: 62–71.

Nisr, C.; Shim, S-H.; Leinenweber, K. & Chizmeshya, A. (2017): Raman spectroscopy of water-rich stishovite and dense high-pressure silica up to 55 GPa. – Am. Mineral., **102**: 2180–2189.

Novák, M. & Cempírek, J. (Eds.) (2010): Granitic pegmatites and mineralogical museums in Czech Republic. – IMA 2010 Field Trip Guide CZ2, 56 p.

Ono, S.; Kikegawa, T.; Higo, Y. & Tange, Y. (2017): Precise determination of the phase boundary between coesite and stishovite in SiO_2. – Phys. Earth Planet. Int., **264**: 1–6.

Rötzler, J.; Hagen, B. &, Hoernes, S. (2008): Geothermometry of the ultrahigh-temperature Saxon granulites revised. Part I: New evidence from key mineral assemblages and reaction textures. – Eur. J. Mineral., **20**: 1097–1115.

Smith, D. C. (1984): Coesite in clinopyroxene in the Caledonides and its implications for geodynamics. – Nature, **310**: 641–644.

Sobolev, N. V.; Fursenko, B. A.; Goryainov, S. V.; Shu, J.; Hemley, R. J.; Mao, H. & Boyd, F. R. (2000): Fossilized high pressure from the Earth's deep interior: The coesite-in-diamond barometer. – Proc. Natl. Acad. Sci. U.S.A., **97**: 11875–11879.

Thomas, R. (2000): Determination of water contents of granitic melt inclusions by confocal laser Raman microprobe spectroscopy. – Am. Mineral., **85**: 868–872.

Thomas, R. & Grew, E. (2021): Coesite inclusions in prismatine from Waldheim, Germany: New constraints on the pressure-temperature evolution of the Saxony Granulite Complex. – Book of Abstracts, 3rd European Mineralogical Conference, EMC 2020, Cracow, Poland, 1 p.

Thomas, R.; Davidson, P.; Rericha, A. & Recknagel, U. (2022): Discovery of stichovite in the prismatine-bearing granulite from Waldheim, Germany: A possible role of supercritical fluids of ultrahigh-pressure origin. – Geosciences, **12**: 196, 1–13.

Thomas, R.; Kamenetsky, V. S. & Davidson, P. (2006): Laser Raman spectroscopic measurements of water in unexposed glass inclusions. – Am. Mineral., **91**: 467–470.

Thomas, S.-M.; Koch-Müller, M.; Reichart, P.; Rhede, D.; Thomas, R.; Wirth, R. & Matsyuk, S. (2009): IR calibration for water determination in olivine, r-GeO_2, and SiO_2 polymorphs. – Phys. Chem. Miner. **36**: 489–509.

Tschauner, O. (2019): High-pressure minerals. – Am. Mineral., **104**: 1701–1731.

Tuschel, D. (2012): Raman crystallography, in theory and practice. – Spectroscopy, **27**(3): 2–6.

Tuschel, D. (2017): Effect of dopants or impurities on the Raman spectrum of the host crystal. – Spectroscopy, **32**(12): 13–19.

Tuschel, D. (2019): Raman spectroscopy and polymorphism. – Spectroscopy, **34**(3), 10–21.

Tuschel, D. (2020): Raman crystallography and the effect of Raman polarizability tensor element values. – Spectroscopy **35**(12): 5–12.

Zagorsky, V. Y. (2007): Deep fluid flow–melt interaction and problems of granite–pegmatite system petrogenesis. – Abstracts in Granitic pegmatites: the state of the art. – Memórias Porto, **8**: 106–107.